EUROPEAN JOURNAL OF PURE AND APPLIED MATHEMATICS
2025, Vol. 18, Issue 3, Article Number 6495
ISSN 1307-5543 – ejpam.com
Published by New York Business Global

Improving Wheelchair Mobility through Enhanced Kalman Filtering

Wael Hosny Fouad Aly[1,*], Nino Samashvili[1], Chadi Fouad Riman[1]

[1] *College of Engineering and Technology, American University of the Middle East, Kuwait*

Abstract. Electric wheelchairs are essential for individuals with lower motor disabilities, enabling daily mobility typically via joystick control. However, users with cerebral palsy often struggle with accurate joystick maneuvering due to motor impairments. This paper proposes a novel control strategy, *Enhanced Kalman Filter-based Wheelchair Control* (**EKFWC**), which compensates for these deficiencies using a Kalman Filter-based estimation model grounded in state-space representations. The system continuously estimates and corrects wheelchair velocity by filtering noisy sensor data and adjusting joystick commands in real time, aligning motion with optimal speeds for varying terrain stored in a reference table. EKFWC's performance is benchmarked against a hybrid sensor fusion model, $\mathbf{REF_{EKFPF}}$, which combines an Extended Kalman Filter and a Modified Particle Filter. Simulation results show that EKFWC yields lower mean absolute error (MAE) and percentage estimation error compared to both EKF and $\text{REF}_{\text{EKFPF}}$. Additionally, EKFWC significantly reduces navigation time: on smooth indoor surfaces, it completes a point-to-point traversal in 71 sec compared to 100 sec for $\text{REF}_{\text{EKFPF}}$; on uneven and very rough outdoor terrains, EKFWC achieves traversal times of 87 sec and 95 sec, respectively. These improvements stem from EKFWC's ability to maintain smoother trajectories with minimal deviation and prompt response to terrain variations, avoiding the zigzagging, wide turns, and hesitations observed in the reference model. Overall, EKFWC demonstrates robust real-time adaptability and enhanced path efficiency across diverse environments.

2020 Mathematics Subject Classifications: 93E11, 68T40, 90B06, 92C50

Key Words and Phrases: Wheelchair Control, Kalman Filters, Mean Absolute Error, Motor Disabilities, Assistive Technologies, Particle Filter, Extended Kalman Filter

1. Introduction

In recent decades, there has been remarkable progress in the development and application of emerging technologies. Among these, robotics has gained a significant presence across various domains, including industry, logistics, mobility, and healthcare. Robots are increasingly capable of assisting humans or replicating human actions in a wide range

*Corresponding author.
DOI: https://doi.org/10.29020/nybg.ejpam.v18i3.6495

Email addresses: wael.aly@aum.edu.kw (W. H. F. Aly),
nino.samashvili@aum.edu.kw (N.Samashvili), chadi.riman@aum.edu.kw (C. F. Riman)

of environments. In particular, robotic assistive devices and mobile robotics—such as smart wheelchairs—offer great potential to enhance the autonomy and daily living of individuals with disabilities and the elderly. A key advancement in this field is the localization of robotic wheelchairs using specialized multi-sensor filters. This sophisticated technique leverages multiple sensors to collect environmental data and applies filtering mechanisms—such as particle filters—to accurately estimate the wheelchair's position within its surroundings. Operating a conventional powered wheelchair can pose substantial challenges for individuals with motor impairments, often making the task difficult or even hazardous. In response, recent research has focused on the development of smart and autonomous wheelchairs capable of compensating for cognitive and perceptual limitations by anticipating obstacles and navigating safely. Notable projects from the past decade include HandiViz [1], Sysiass [2], Coalas [3], NavChair [4], and the EU-funded FP7 Radhar [5].

Recent advancements in estimation, adaptive control, and intelligent decision-making have inspired robust approaches for real-time systems operating in uncertain environments. In assistive technologies, probabilistic modeling has proven effective for handling noisy physiological signals. Safi et al. [6] applied a Hidden Markov Model to balance data from Parkinson's patients, emphasizing the value of model-based estimation for user state prediction—an approach conceptually aligned with our Kalman filter-based correction model. In a similar vein, Kanj et al. [7] and Kanj et al. [8] introduced dynamic, agent-based risk models for transportation, demonstrating the effectiveness of distributed, state-aware simulation in high-risk control environments. Trust and fairness in task distribution under uncertainty have also been studied in multi-provider systems. Al-Tarawneh et al. [9] proposed an MCDM framework for trust-aware task offloading in heterogeneous edge-fog-cloud networks, showcasing adaptive strategies that are analogous to our real-time terrain-dependent velocity adjustments. In the domain of networked systems, Aly et al. [10] developed an unbound machine learning architecture for SDN controllers, while Aly et al. [11] introduced dynamic feedback mechanisms for optimal controller placement—both aligning with our use of feedback correction loops for joystick input filtering. Spatial optimization under constraints, a principle vital to efficient navigation, was explored by Danach et al. [12], who proposed UAV-based service placement strategies during crisis conditions. Their terrain-aware spatial modeling complements our use of a reference table for terrain-specific speed adaptation. Additionally, low-latency and low-complexity algorithmic design has been emphasized in wireless systems by Alabed et al. [13], where a differential scheme using space-time block coding was introduced to minimize decoding overhead—an optimization trade-off relevant to embedded wheelchair control systems. Complementing these efforts, data-driven approaches for semantic inference and classification have been advanced by Al-Tarawneh et al. [14], who utilized word embeddings in a hybrid learning model for fake news detection, emphasizing real-time signal interpretation. Mahariq et al. [15] applied spectral element methods to study acoustojets, highlighting the growing use of physics-inspired, mesh-based numerical modeling, which supports the adoption of state-space modeling techniques in control applications like our proposed EKFWC framework.

Each project has contributed uniquely to the advancement of smart wheelchair technologies. For instance, the Sysiass project employed EMG and camera sensors; however, its obstacle detection and stopping mechanisms lacked sufficient precision unless the wheelchair was perfectly aligned. HandiViz addressed this by integrating 15 ultrasonic sensors around the wheelchair, enabling real-time trajectory correction through an innovative obstacle avoidance and control system that merged user input with autonomous navigation. Meanwhile, NavChair utilized GPS, compass, and ultrasonic sensors, but faced limitations in map tracking and localization accuracy due to the imprecision of its calculations. Errors in determining the robot's position and orientation remained significant challenges.

The rest of this paper is organized as follows: Section 2 provides a literature review with a reference model used for comparison with our proposed model. Section 3 has the reference model. Section 4 details the proposed controller's model, including the mathematical framework and overall system design. Section 5 presents the simulation testbed and results. Section 6 concludes the paper and discusses the future work.

2. Literature Review

The literature reflects extensive efforts toward designing the next generation of intelligent wheelchairs [16]. From a technological standpoint, research has incorporated a variety of assistive tools—such as ultrasound, laser range finders, and vision-based sensors—along with sophisticated algorithms for data processing. Today, the topic occupies a central role in mobile robotics, integrating advancements in artificial intelligence, user interaction, human learning, localization, multi-modal sensors, and adaptive systems tailored to users' specific abilities and limitations [5].

Despite promising developments, significant scientific challenges persist, especially in effectively integrating diverse technological components [17–19]. Localization and navigation remain among the most critical issues in the development of smart mobile robots [20, 21]. A core challenge lies in achieving robust data fusion from various sensors and devices through reliable computational methods, enabling accurate self-localization and intuitive interaction with users under both autonomous and semi-autonomous modes [22, 23]. High precision and reliability are particularly vital for user safety in smart wheelchair localization systems, especially within indoor environments such as homes, hospitals, and commercial centers [24].

Indoor localization is complicated by structural variability and dynamic obstacles, making accurate positioning essential to prevent collisions and support smooth navigation [25, 26]. Even minor localization errors can compromise user safety. Furthermore, wheelchairs operating outdoors must contend with added complexities such as uneven terrain, environmental interference, and variable weather conditions [16, 17]. These factors necessitate advanced adaptive localization systems [27].

Localization is a cornerstone for achieving full autonomy in mobile robotics. Gasparri et al. [28] proposed a global localization strategy that combines particle filtering with extended Kalman filters. Their hybrid approach begins with a particle filter generating

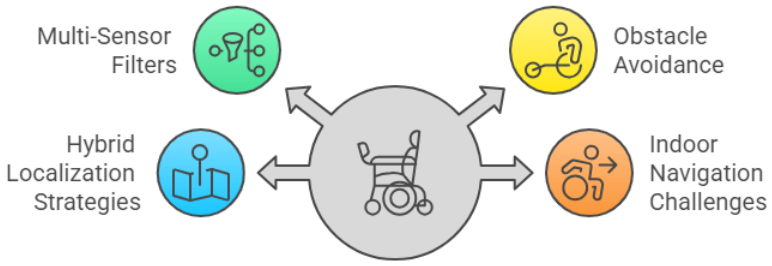

Figure 1: Smart Wheelchair Localization Navigation

pose hypotheses under stationary conditions, followed by planned motion to reduce uncertainty. Parallel EKFs then validate these hypotheses without relying on feature-based landmarks, allowing for a more flexible environmental model. Another hybrid strategy involves wireless sensor networks (WSNs), as demonstrated by Achroufene et al. [29]. Their method incorporates belief function theory to address imperfections in received signal strength (RSS) measurements and the credibility of data sources. It also models signal disparities caused by intrusion and attenuation, which are common challenges in indoor environments.

The Extended Kalman Filter (EKF) remains a widely used algorithm for estimating nonlinear systems, prized for its simplicity, computational efficiency, and generally reliable results. In a hybrid approach known as the Extended Kalman Particle Filter (EKPF), particles are sampled from the probability distribution function generated by EKF rather than from the system's transition model [30]. This method combines the strengths of EKF (rapid initial estimation) and particle filters (robustness to nonlinearity and non-Gaussian noise). The specific design of such hybrid algorithms depends on application needs and system characteristics. These approaches are particularly attractive due to their low cost and effectiveness, requiring fewer external sensors or infrastructure such as beacons. Regression techniques are used [11, 31, 32].

The present work addresses localization and navigation challenges in smart wheelchairs through a Hybrid Filter (HF)-based multi-sensor data fusion framework. The proposed method seeks to reduce estimation errors and enhance system accuracy in indoor environments. The performance and practical applicability of the approach are demonstrated through simulations, with the results benchmarked against existing methods in the literature as shown. Smart Wheelchair Localization Navigation is shown in Figure 1.

The $KalmanFilter(KF)$ is widely recognized as a robust and efficient algorithm for data fusion and filtering, with extensive applications across numerous research domains, particularly in mobile robotics [33–35]. By design, the classical KF is suitable for systems characterized by linear dynamics. However, many real-world robotic systems involve nonlinearities in either the process model, the measurement model, or both.

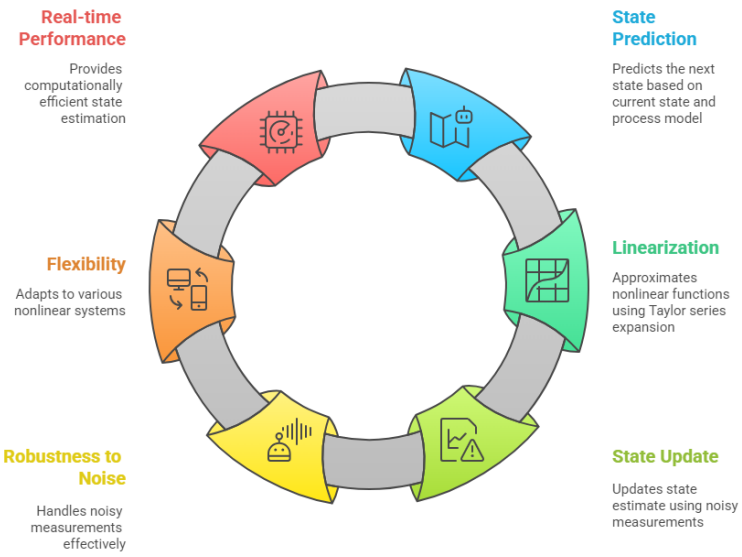

Figure 2: Components of the Extended Kalman Filter

To accommodate such complexities, the $ExtendedKalmanFilter(EKF)$ is employed, incorporating a linearization step to approximate the nonlinear system behavior [35]. This is typically achieved through a first-order Taylor series expansion, which allows the nonlinear functions to be treated within a linear framework. The EKF is capable of providing accurate state estimates from noisy measurements, under the assumption that the measurement noise is Gaussian, zero-mean, temporally uncorrelated, and of known variance. A conceptual overview of the localization approach using EKF is illustrated in Figure 2.

3. REF_{EKFPF} Reference Model

In this work, we adopt the model proposed by Meddeber et al. [36] as the reference framework for evaluating our proposed system. This reference model will be denoted as REF_{EKFPF} throughout this article.

The REF_{EKFPF} model is designed to support intelligent wheelchair navigation through the implementation of a multi-sensor data fusion mechanism based on a hybrid filtering (HF) strategy. Specifically, REF_{EKFPF} integrates the strengths of the Extended Kalman Filter (EKF) and the Particle Filter (PF) to address the challenges associated with nonlinear system dynamics and sensor uncertainty. The hybrid approach aims to reduce estimation errors and improve the accuracy of dynamic localization, particularly in structured indoor environments. The system leverages odometry and

laser rangefinder data to estimate the wheelchair's position and orientation in real-time, achieving enhanced tracking precision compared to traditional single-filter techniques.

Simulation results presented in the original study demonstrate that REF_{EKFPF} outperforms conventional EKF and standalone PF methods in terms of mean absolute error (MAE) and percentage estimation error. The model provides a foundation for autonomous navigation in assistive mobility devices, seeking to offer a reliable and efficient localization solution tailored for individuals with reduced mobility. However, several limitations are noted. The validation of the system is confined to simulation, with limited testing in real-world environments and no involvement of actual users. As a result, the generalizability and practical usability of the model remain uncertain. Moreover, the framework focuses primarily on low-level navigation tasks without incorporating user interaction or adaptive control strategies. The reliance on a simplified two-wheel kinematic model constrains the applicability to other wheelchair configurations, and the computational overhead introduced by advanced filters such as the Unscented Kalman Filter (UKF) and Adaptive Kalman Filter (AKF) is not sufficiently addressed. Additionally, the adaptive tuning mechanism for the AKF lacks a well-defined procedure for adjusting noise parameters under dynamic conditions, which may affect real-time feasibility and robustness.

4. $EKFWC$ Proposed Model

The proposed model used in this work is based on Kalman filters. The Kalman Filter is a recursive algorithm used for estimating the state of a dynamic system from noisy measurements. It operates in two main steps: prediction and correction. In the prediction step, it uses the system model to estimate the current state and the uncertainty (error covariance). In the correction step, the Kalman Filter adjusts the predicted state by incorporating new measurements and a calculated Kalman gain, which determines how much weight should be given to the new measurements. This iterative process reduces the error in state estimation over time, making it particularly effective for systems with uncertainty and noise, such as navigation, robotics, and control systems.

4.1. Wheelchair System Identification

The power wheelchair utilizes batteries to control a direct drive system. The Wheelchair joystick controller has a linear relationship between the force applied and the motor speed or angular velocity. A force feedback joystick typically operates between 0 to 15 mNm (milli-newton meters).

The following formulas convert joystick input values y_{input} (vertical joystick movement) and x_{input} (horizontal joystick movement) into physical movement parameters Υ (linear speed) and θ (angular speed):

$$\Upsilon = \frac{y_{\text{input}} - \overline{y}}{\overline{y}} \times \Upsilon_{\max}, \tag{1}$$

$$\theta = \frac{x_{\text{input}} - \overline{x}}{\overline{x}} \times \theta_{\max}, \tag{2}$$

where $\overline{x}$ and $\overline{y}$ are assumed to be equal to 7.5.

Table 1 shows the numerical relation between the joystick input and the speed of a wheelchair, assuming that the maximum speed that the wheelchair can achieve is $\Upsilon_{\max} = 60\,\text{cm/s}$ and the maximum turning angle is $\theta_{\max} = 30°$, which is a reasonable limit for wheelchair turning.

Table 1: Joystick input vs. speed and turning angle.

Joystick Input I	**Normalized Value** μ	**Speed Output** Υ **(cm/s)**	**Turning Angle Output** θ **(°/s)**
0	-1	-60	-30.0
2.5	-0.67	-40.2	-20.1
5	-0.33	-19.8	-9.9
7.5	0	0	0
10	0.33	19.8	9.9
12.5	0.67	40.2	20.1
15	1	60	30.0

Equations governing the wheelchair's speed and angular velocity are given in equations 3 and 4 respectively.

$$\omega_t = A_\omega\, \omega_{t-1} + B_\omega\, u_\omega, \tag{3}$$

$$v_t = A_s\, v_{t-1} + B_s\, u_s. \tag{4}$$

where v_t and ω_t represent the speed and angular velocity at time t, respectively. A_s and A_ω are the state coefficients affecting speed and angular velocity. B_s and B_ω are the control input coefficients for speed and angular velocity. u_s and u_ω are the joystick input values for speed and turning. In the current model, parameters such as A_s and Q_s are selected based on expected behavior of the wheelchair on various surface types. Typical values of A_s are shown in Table 2. Typical values of Q_s are shown in Table 3.

Choosing an appropriate value of A_s is important to improve the accuracy of speed prediction in a Kalman filter model. Surfaces with lower resistance maintain speed better between steps, resulting in higher A_s values. Q_s represents the process noise covariance and may be derived experimentally or estimated from manufacturer-provided motor controller data. Higher Q_s values indicate less confidence in the model's prediction due to unstable surface behavior.(Thrun et al. [37], Iagnema et al. [38], Reister, D. B et al [39], Barfoot, T. D. [40].)

In the state prediction step, we use the Kalman Filter prediction equation:

$$X_t = FX_{t-1} + BU_t, \tag{5}$$

Table 2: Typical A_s Values and Descriptions for Different Surface Types

Surface Type	**Estimated A_s**	**Description**
Indoor Smooth Floor (e.g., tiles, polished concrete)	0.95 – 0.99	Very low resistance; speed is mostly maintained.
Outdoor Uneven Surface (e.g., pavement, grass, gravel)	0.70 – 0.90	Moderate resistance; speed decreases more between steps.
Very Rough Outdoor Surface (e.g., sand, rocky terrain)	0.30 – 0.70	High resistance; speed reduces significantly each step.

Table 3: Typical Values of Q_s Based on Terrain Conditions

Surface Description	**Range of Q_s**	**Remarks**
Indoor Smooth	0.01 – 0.1	Use small values if the system is relatively stable and fluctuations are minimal.
Outdoor Uneven	0.1 – 0.5	Moderate noise due to bumps, irregular ground, or mixed surfaces.
Very Rough Outdoor	> 0.5	High uncertainty; rough terrain introduces large speed fluctuations.

where

$$X_t = \begin{bmatrix} v_t \\ \omega_t \end{bmatrix}, \quad X_{t-1} = \begin{bmatrix} v_{t-1} \\ \omega_{t-1} \end{bmatrix}. \tag{6}$$

The state transition matrix is:

$$F = \begin{bmatrix} A_s & 0 \\ 0 & A_\omega. \end{bmatrix}$$

The control input matrix is:

$$B = \begin{bmatrix} B_s & 0 \\ 0 & B_\omega \end{bmatrix}, \quad U_t = \begin{bmatrix} u_s \\ u_\omega \end{bmatrix}.$$

Error covariance prediction equation is:

$$P_t = FP_{t-1}F^T + Q, \tag{7}$$

where

$$P_{t-1} = \begin{bmatrix} P_{s,t-1} & 0 \\ 0 & P_{\omega,t-1} \end{bmatrix}, \quad Q = \begin{bmatrix} Q_s & 0 \\ 0 & Q_\omega \end{bmatrix}.$$

Here, $P_{s,t-1}$ is the previous error covariance for the speed, representing how much we trust our previous speed estimate. This value is updated at each iteration of the Kalman Filter.

To compute variance we have:

$$P_{s,t-1} = \frac{1}{N}\sum_{i=1}^{N}(\upsilon_i - \overline{\upsilon})^2, \tag{8}$$

where υ_i are past speed sensor measurements and $\overline{\upsilon}$ is the average speed.

The Kalman gain is computed as follows:

$$K = P_t H^T (H P_t H^T + R)^{-1}, \tag{9}$$

where

$$H = \begin{bmatrix} h_{11} & h_{12} \\ h_{21} & h_{22} \end{bmatrix}$$

and

$$R = \begin{bmatrix} R_s & 0 \\ 0 & R_\omega \end{bmatrix}.$$

Elements of H are determined based on how the sensors map to the actual states and R_s reflects the noise level (or uncertainty) in speed sensor measurements. These uncertainties may vary depending on environmental factors, such as roughness or terrain vibrations. In this work, we assume H as identity for simplicity, implying direct measurement of both speed and angular velocity. In this paper, we do not use real sensor data but instead assume idealized measurements for speed and angular velocity. These assumed measurements serve as the basis for state updates in the Kalman filter equations.

The updated speed and angular velocity are obtained by using:

$$X = X_t + K(Z - HX_t), \tag{10}$$

where Z is the observed measurement vector:

$$Z = \begin{bmatrix} z_s \\ z_\omega \end{bmatrix}.$$

The updated error covariance is:

$$P = (I - KH)P_t, \tag{11}$$

where I is the identity matrix:

$$I = \begin{bmatrix} 1 & 0 \\ 0 & 1 \end{bmatrix}$$

These equations form the basis of the EKFWC model, enabling adaptive real-time correction of wheelchair motion based on terrain-dependent dynamics and sensor estimates.

4.2. Scenario Description and Analysis Setup

We consider the following scenario to evaluate the performance of the Kalman Filter under varying joystick inputs and surface conditions: The wheelchair begins by moving forward at an initial speed of 8 cm/s. To increase its velocity, normalized value of a joystick input $\mu_{s1} = 0.3333333$ is applied, followed by a further acceleration using $\mu_{s2} = 0.6666667$. The wheelchair then slightly reduces its speed and initiates a right turn with inputs $\mu_{s3} = 0.3333333$ and $\mu_{\omega 1} = 0.3333333$. Subsequently, it performs two consecutive left turns without altering its speed, using angular velocity inputs $\mu_{\omega 2} = -0.66666667$ and $\mu_{\omega 3} = -0.3333333$. Finally, the wheelchair resumes forward motion, gradually increasing its speed with $\mu_{s4} = 0.6666667$, and ultimately reaches the maximum input of $\mu_{s5} = 1.0$.

The Kalman Filter will be applied to three different surface types to analyze the impact of terrain-induced uncertainty:

(i) Indoor Smooth Surface

(ii) Outdoor Uneven Surface

(iii) Very Rough Outdoor Surface

To evaluate the prediction and update process of the Kalman Filter under varying terrain conditions, we consider the following joystick input sequence:

Table 4: Joystick Inputs for Speed and Turning

Step	**Speed Input** u_s	**Angular Input** u_ω
1	0.3333333	0
2	0.6666667	0
3	0.3333333	0.3333333
4	0.3333333	-0.6666667
5	0.3333333	-0.3333333
6	0.6666667	0
7	1.0000000	0

The wheelchair begins with the following.

- Previous speed: $v_{t-1} = 8\,\text{cm/s}$
- Previous angular velocity: $\omega_{t-1} = 0^\circ/\text{s}$
- Control input coefficients: $B_s = 60\,\text{cm/s}, \quad B_\omega = 30^\circ/\text{s}$

The performance of the Kalman Filter heavily depends on the careful selection of its initial parameters. Specifically, the initial state vector is typically set based on prior knowledge of the system's starting position, velocity, and orientation. $EKFWC$ used

Table 5: Initial Data for Speed Prediction

Parameter	**Indoor Smooth**	**Outdoor Uneven**	**Very Rough Outdoor**
A_s (Speed Coefficient)	0.9	0.6	0.4
$P_{s,t-1}$ (Error Covariance)	0.03	0.04	0.05
Q_s (Process Noise Cov.)	0.05	0.10	0.60
R_s (Measurement Noise Cov.)	0.02	0.30	0.50

Table 6: Initial Data for Angular Velocity Prediction

Parameter	**Indoor Smooth**	**Outdoor Uneven**	**Very Rough Outdoor**
A_ω (Angular Coefficient)	0.9	0.5	0.3
$P_{\omega,t-1}$ (Error Covariance)	0.06	0.07	0.08
Q_ω (Process Noise Cov.)	0.02	0.10	0.60
R_ω (Measurement Noise Cov.)	0.01	0.30	0.50

the speed parameters listed in table 5. The EKFWC utilized the angular velocity parameters detailed in Table 6, which were essential for accurately modeling the wheelchair's rotational dynamics and ensuring responsive control during turning maneuvers.

This setup serves as a simulation scenario for validating the dynamic response of the Kalman Filter. While the coefficients and noise covariances are not obtained from hardware sensors, they reflect reasonable operating ranges found in prior robotic mobility studies. This approach allows us to focus on how terrain-induced uncertainty affects filter stability and correction.

4.3. Kalman Filter Application and Stepwise Observations

To analyze the impact of different types of surfaces on wheelchair movement, we applied Kalman Filter iteratively after each joystick input step. The calculations provide predictions for speed and angular velocity, Kalman gains, corrections based on observed measurements, and updated error covariances. In this study, the Kalman Filter is applied iteratively to refine speed and angular velocity estimations for a wheelchair that navigates different terrain conditions. The filter updates its predictions based on process and measurement noise, incorporating Kalman gains to correct errors and improve accuracy. Each iteration consists of a prediction step, where the speed and angular velocity of the wheelchair are estimated, followed by a correction step that adjusts these values based on observed measurements.

In the context of wheelchair motion, angular velocity ω denotes the rate and direction of turning. Positive values indicate right turns, while negative values correspond to left turns. These negative values are expected and essential for accurately capturing directional changes in trajectory.

Step 1: Initial phase The wheelchair begins to move with an initial speed of 8 cm/s no angular velocity. A joystick input of 0.3333333 is applied. The Kalman Filter

predicts the speed for each surface type based on the system model, and then updates it using the Kalman gain and measurement data. The Kalman Gains (K_s, K_ω) are high (close to 1), meaning the filter places significant trust in the measurement.

Step 2: Further speed increase

The wheelchair continues accelerating with a new joystick input of 0.6666667. The predicted speed reaches 60 cm/s for Indoor Smooth surfaces, with a Kalman gain of 0.4407, leading to a corrected speed of 59.5593 cm/s. The Kalman gains are lower compared to the first step, showing that the filter is becoming more confident in its estimates. On indoor smooth surface, lower K_s (0.44) shows the prediction is stable; less correction is needed. Outdoor uneven, gains are moderate, correction shifts the prediction closer to the measurement. On a very rough surface gains (0.35) show that even with high noise, the model is adjusting more conservatively compared to Step 1.

Step 3: Introduction of Angular Velocity At this step, the wheelchair starts turning right while slightly reducing speed. The joystick input for speed is 0.3333333, and for angular velocity it is 0.3333333. The Kalman Filter adapts to track both linear and angular components. On smooth surfaces, the gains are slightly reduced compared to straight motion due to additional angular uncertainty.The predicted speed remains 60 cm/s for Indoor Smooth surfaces, with a Kalman gain of 0.3059, leading to an updated speed of 59.6941 cm/s. The predicted angular velocity is 10°/s, corrected to the same value after filtering. On Outdoor Uneven surfaces, the predicted speed is 52.7515 cm/s, adjusted to 52.6178 cm/s, while for Very Rough Outdoor terrain, it is 39.4626 cm/s, adjusted to 39.0799 cm/s. A turning motion is introduced with an angular velocity input. The Kalman Filter now processes both speed and angular velocity predictions. The filter updates the angular velocity effectively, maintaining a balance between prediction and correction. The error covariance values continue to decrease, showing improved accuracy in the estimation. The rougher surfaces again exhibit higher discrepancies between prediction and correction.

Step 4 and 5: Consecutive Left Turns Two consecutive left turns are applied without changing the speed. The filter efficiently processes the angular velocity changes while ensuring stability in speed estimation. The predictions and corrections remain consistent across surface types, with rougher surfaces still showing slightly larger deviations. The Kalman gains for angular velocity slightly decrease, indicating improved confidence in turn estimations. Low gains show the model is very confident in its state estimation.

Step 6 and 7: Gradual Speed Increase and Maximum Speed Application The wheelchair accelerates again, moving towards its maximum speed. The Kalman Filter continues refining its estimates, and the correction step brings the speed closer to the prediction. The updated error covariance values are now quite low, indicating a high level of certainty in both the speed and the angular velocity estimates. The filter effectively accounts for varying surface conditions, maintaining accuracy even in more complex scenarios. Finally, the wheelchair reaches its highest speed with a joystick input of 1.0. The predicted speed is 60 cm/s for all surfaces, with corrected speeds are close to the predicted ones. The final corrected angular velocities are -16.125°/s, -4.3619°/s,

and -1.33°/s, respectively. The updated error covariances indicate improved confidence in the estimated values after applying the Kalman Filter at each step. The Kalman Filter predictions are now highly accurate, and the correction step only slightly refines the values. The error covariance values are at their lowest, showing that the filter has fully adapted to the system dynamics.

Table 7: Kalman Filter Results – Step 1

Surface Type	**Pred Speed**	**Pred** ω	K_s	K_ω	**Corr Speed**	**Corr** ω	$\hat{P}_s$	$\hat{P}_\omega$
Indoor Smooth	27.20	0	0.7879	0.8728	27.04	0	0.0158	0.0087
Outdoor Uneven	24.80	0	0.2761	0.2814	24.58	0	0.0828	0.0844
Very Rough Outdoor	23.20	0	0.5487	0.5484	22.54	0	0.2744	0.2742

where $\hat{P}_s$ and $\hat{P}_\omega$ denote the updated error covariance for speed and angular velocity, respectively.

Table 8: Kalman Filter Results – Step 2

Surface Type	**Pred Speed**	**Pred** ω	K_s	K_ω	**Corr Speed**	**Corr** ω	$\hat{P}_s$	$\hat{P}_\omega$
Indoor Smooth	60.00	0	0.4407	0.4660	59.56	0	0.0088	0.0047
Outdoor Uneven	54.75	0	0.2163	0.2196	54.59	0	0.0649	0.0659
Very Rough Outdoor	49.02	0	0.3543	0.3542	48.66	0	0.1772	0.1771

Table 9: Kalman Filter Results – Step 3: Turning Begins

Surface Type	**Pred Speed**	**Pred** ω	K_s	K_ω	**Corr Speed**	**Corr** ω	$\hat{P}_s$	$\hat{P}_\omega$
Indoor Smooth	60.00	10.00	0.3059	0.3179	59.69	10.00	0.0061	0.0032
Outdoor Uneven	52.75	10.00	0.1779	0.1801	52.62	10.00	0.0534	0.0540
Very Rough Outdoor	39.46	10.00	0.2616	0.2615	39.08	10.00	0.1308	0.1308

Visual representation of how the Kalman Gain (K_s) and the error covariance ($\hat{P}_s$) for speed evolve across the steps for each surface type: Left Plot (Kalman Gain - K_s) shows that the Kalman Gain decreases with each step, indicating that the filter becomes more confident in its prediction as it incorporates more data. Right Plot (Error Covariance - s) also decreases steadily, demonstrating that the uncertainty in the speed estimate is reducing with each iteration—highlighting the filter's effectiveness.

The graph in Figure 4 represents how the Kalman Gain for angular velocity (K_ω) and the updated error covariance ($\hat{P}_\omega$) evolve over the 7 steps.

K_ω and $\hat{P}_\omega$ decrease step-by-step for all surfaces, indicating that the Kalman filter gradually puts more trust in its internal model as the uncertainty reduces.

Table 10: Kalman Filter Results – Step 4: Sharp Turn and Reduced Speed

Surface Type	**Pred Speed**	**Pred** ω	K_s	K_ω	**Corr Speed**	**Corr** ω	$\hat{P}_s$	$\hat{P}_\omega$
Indoor Smooth	60.00	-11.00	0.2342	0.2412	59.77	-11.00	0.0047	0.0024
Outdoor Uneven	51.57	-15.00	0.1510	0.1526	51.48	-15.00	0.0453	0.0458
Very Rough Outdoor	35.63	-17.00	0.2074	0.2073	35.50	-17.00	0.1037	0.1037

Table 11: Kalman Filter Results – Step 5: Sharpest Turn

Surface Type	**Pred Speed**	**Pred** ω	K_s	K_ω	**Corr Speed**	**Corr** ω	$\hat{P}_s$	$\hat{P}_\omega$
Indoor Smooth	60.00	-19.90	0.1898	0.1943	59.81	-19.92	0.0038	0.0019
Outdoor Uneven	50.89	-17.50	0.1312	0.1324	50.77	-17.57	0.0394	0.0397
Very Rough Outdoor	34.20	-15.10	0.1718	0.1717	33.99	-15.08	0.0859	0.0859

$EKFWC$ proposed model algorithm is given in algorithm 1.

Table 12: Kalman Filter Results – Step 6: Recovery and Slowing Turn

Surface Type	**Pred Speed**	**Pred** ω	K_s	K_ω	**Corr Speed**	**Corr** ω	$\hat{P}_s$	$\hat{P}_\omega$
Indoor Smooth	60.00	-17.93	0.1595	0.1627	59.84	-17.94	0.0032	0.0016
Outdoor Uneven	60.00	-8.78	0.1160	0.1169	59.88	-8.81	0.0348	0.0351
Very Rough Outdoor	53.60	-4.52	0.1466	0.1466	53.51	-4.59	0.0733	0.0733

Table 13: Kalman Filter Results – Step 7: Stabilizing Trajectory

Surface Type	**Pred Speed**	**Pred ω**	K_s	K_ω	**Corr Speed**	**Corr ω**	$\hat{P}_s$	$\hat{P}_\omega$
Indoor Smooth	60.00	-16.15	0.1376	0.1399	59.86	-16.13	0.0028	0.0014
Outdoor Uneven	60.00	-4.40	0.1039	0.1047	59.90	-4.36	0.0312	0.0314
Very Rough Outdoor	60.00	-1.38	0.1278	0.1278	59.87	-1.33	0.0639	0.0639

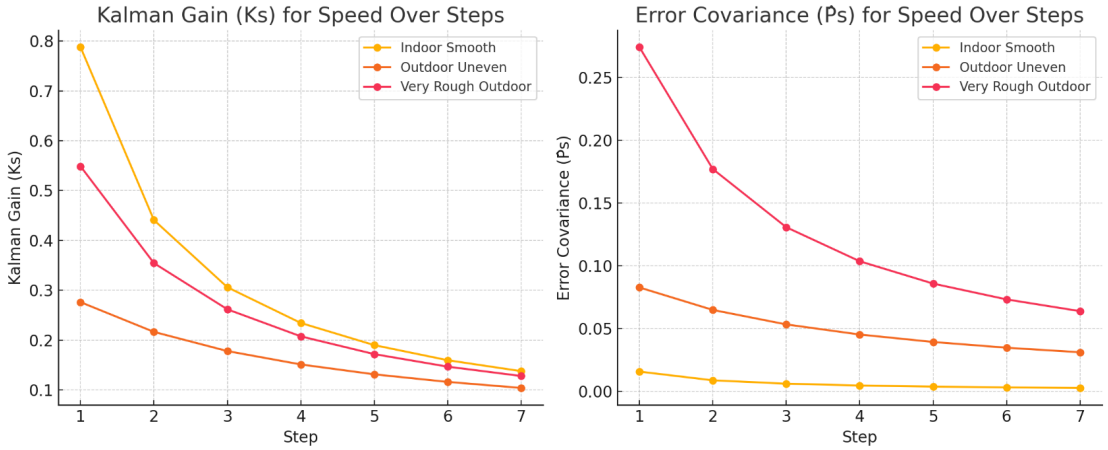

Figure 3: Kalman Gain (K_s) and the error covariance ($\hat{P}_s$)

Algorithm 1 Kalman Filter for Wheelchair Speed and Angular Velocity Estimation

Inputs:

z_s, z_ω — Measured speed and angular velocity

u_s, u_ω — Joystick input values for speed and turning

Parameters:

A_s, A_ω — State coefficients for speed and angular velocity

B_s, B_ω — Control input coefficients

Q_s, Q_ω — Process noise covariances

R_s, R_ω — Measurement noise covariances

Δt — Time step duration

Output:

v_t, ω_t — Estimated speed and angular velocity

1: **procedure** KALMAN_SPEED_ESTIMATION(z_s, z_ω, u_s, u_ω)

2: **Initialization:** Set initial state estimates: v_0, ω_0 Set initial error covariances: $P_{s,0}$, $P_{\omega,0}$

3: Define system matrices A, B, H, process noise covariance Q, and measurement noise covariance R.

4: **Prediction Step:** Predict speed and angular velocity using (5).

5: **Correction Step**: Compute Kalman gain: equations (9)

6: **Update step** Update speed, angular velocity, error covariance (10) and (11). Update sensor values and return to prediction step.

7: **end procedure**

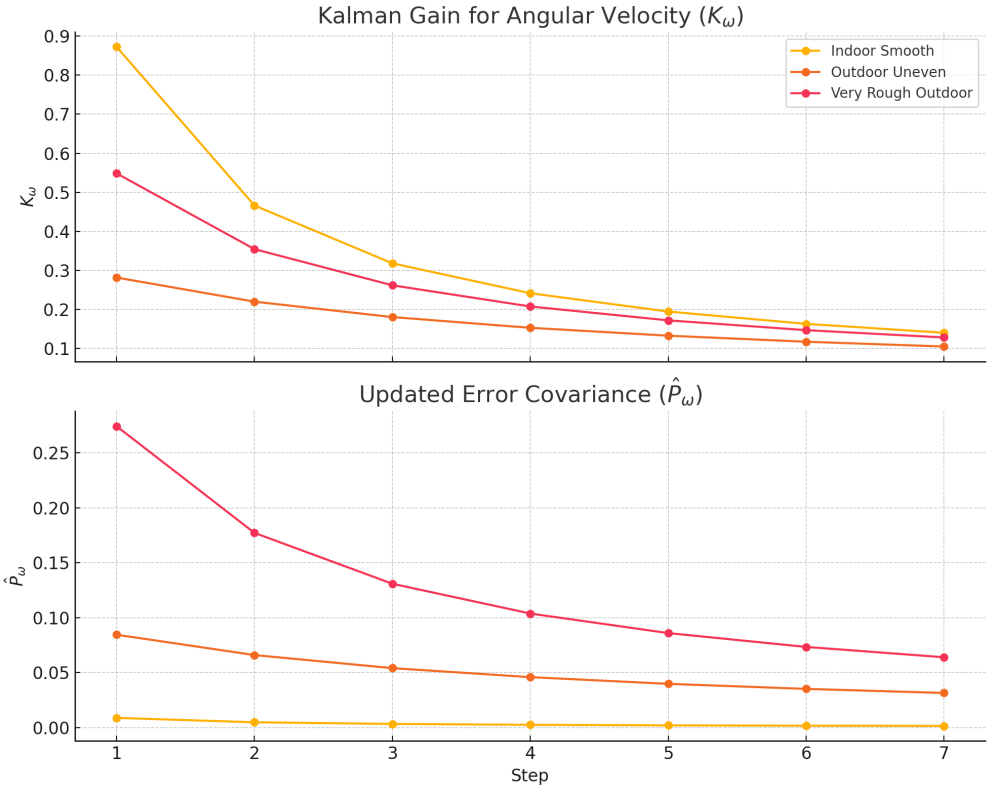

Figure 4: Kalman Gain (K_ω) and the error covariance ($\hat{P}_\omega$)

5. Experimental Testbed and Results

In this section, experimental testbed and results will be discussed.

5.1. Experimental Testbed

In this work we assume that the state of the robot is defined by its position in the $2D$ plane (x, y) and its orientation angle θ. The continuous-time kinematic model maps the linear and angular velocities to the rate of change in position and orientation as follows:

$$\dot{x} = v\cos(\theta) \tag{12}$$

$$\dot{y} = v\sin(\theta) \tag{13}$$

$$\dot{\theta} = \omega \tag{14}$$

For computational applications, especially in control and simulation, the above equations are discretized using Euler integration over a small time step Δt:

$$x_{t+1} = x_t + v\cos(\theta_t)\Delta t \tag{15}$$

$$y_{t+1} = y_t + v\sin(\theta_t)\Delta t \tag{16}$$

$$\theta_{t+1} = \theta_t + \omega \Delta t \tag{17}$$

The linear and angular velocities can also be derived from the individual wheelchair speed. Let r be the radius of each wheel, L be the distance between the wheels (wheelbase),ω_L and ω_R be the angular velocities of the left and right wheels respectively. The linear and angular velocities of the robot can then be computed as:

$$v = \frac{r}{2}(\omega_R + \omega_L) \tag{18}$$

$$\omega = \frac{r}{L}(\omega_R - \omega_L) \tag{19}$$

To test the proposed Kalman model, a simulation software was developed using the C# programming language within the Microsoft Visual Studio environment. The system was executed on an HP machine equipped with an Intel Core $i5$-4590S CPU running at 3.00 GHz and 8 GB of RAM, operating under *Windows 10 Pro* (version 1709, 64-bit). The software, named *Kalman Navigation*, utilizes a 10 m $\times$ 10 m grid containing several obstacle walls and a circular object, as shown in Figure 5(a).

The simulator allows users to input Kalman filter coefficient parameters for both linear and angular velocity. For linear speed, the parameters include: A_s, B_s, $P_s(t-1)$, Q_s, R_s, and $V(t-1)$. For angular velocity, the parameters are: A_w, B_w, $P_w(t-1)$, Q_w, R_w, and $W(t-1)$. Users can choose from preset terrains: *Indoor Smooth*, *Outdoor Uneven*, and *Outdoor Rough*.

The maximum linear speed is set to 60 cm/s, and the maximum angular speed is 30 rad/s. The initial linear speed $V(t-1)$ is set to 8 cm/s, and the angular velocity to 0 rad/s, both of which can be modified by the user. The simulation includes an option to load a predefined scenario consisting of multiple steps with varying linear and angular speeds. Additionally, the system provides functionality to load previously saved test data and visualize the results on the grid.

5.2. Experimental Results

In order to evaluate the proposed model, three sets of experiments were conducted with various Kalman filter parameters for both linear and angular velocities. The three different sets of parameters are shown in table 1. The blank grid that has the terrain we used to conduct the experiments for various scenarios is shown in figure 5(a).

The *EKFWC* simulation package we developed was evaluated on a blank navigation terrain, as illustrated in Figure 5(b).

In this work we conducted three navigation experiments on three different surfaces. In all the experiments, the wheelchair starts from point A till it reaches back to point E. Figure 6(a) has the navigation over an indoor smooth surface, while figure 6(b) has the outdoor uneven terrain. Figure 6(c) has the navigation over an outdoor rough terrain. Figure 6(d) assembles the results over three surfaces to compare the behavior for each scenario.

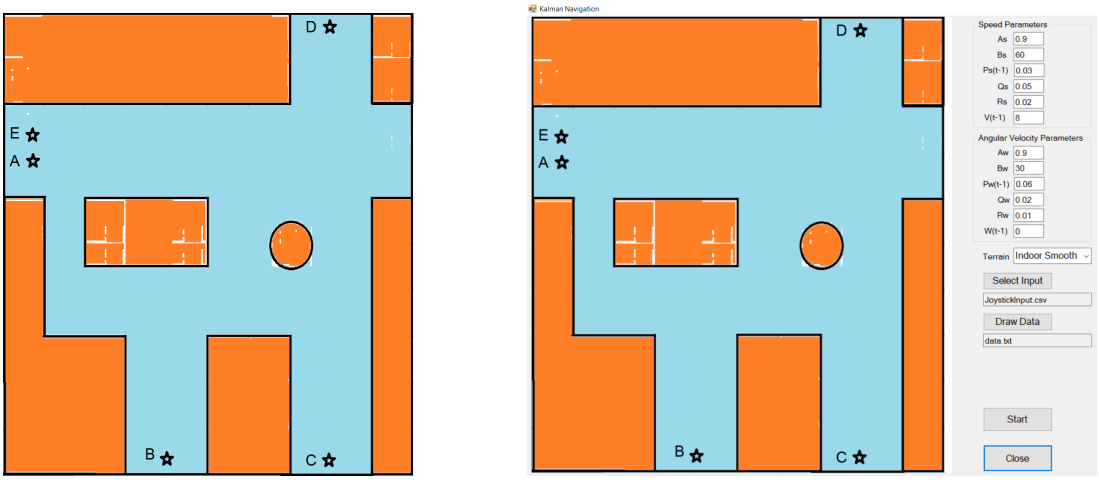

(a) Blank Grid (b) Software

Figure 5: Empty Grid and Software package

The REF_{EKFPF} reference model uses the extended Kalman filter (EKF) and the modified particle filter (PF). Figure 7 has the navigation of the reference model REF_{EKFPF} in the experimental navigation field. In figure 8(a), we compare the proposed $EKFWC$ to the reference REF_{EKFPF} results in a smooth indoor surface environment. Figure 8(b) compares the proposed $EKFWC$ to the REF_{EKFPF} to a smooth indoor surface environment. Figure 8(c) compares the proposed $EKFWC$ to the reference REF_{EKFPF} in an outdoor uneven surface environment. Figure 8(d) compares the proposed $EKFWC$ to the reference REF_{EKFPF} in an outdoor very rough surface environment. Results show that the $EKFWC$ outperforms REF_{EKFPF} in terms of smooth navigation without hitting obstacles on the way starting from point A till it returns back to point E passing all the intermediate navigation points B, C, D. A differential-drive robot is a non-holonomic system equipped with two independently driven wheels. The robot's motion is characterized by Linear velocity(v): the forward or backward motion of the robot and angular velocity(ω): the rotational rate around the vertical axis (yaw).

Figures 9, 10, and 11 illustrate the evolution of the mean absolute errors (MAE) in the wheelchair's estimated position and orientation over time. Specifically, Figure 9 presents the variation in the MAE of the x-coordinate, Figure 10 shows the corresponding error in the y-coordinate, and Figure 11 depicts the error in the orientation angle θ. These plots provide insight into the estimation accuracy of the proposed $EKFWC$ system and highlight its ability to maintain low tracking error throughout the navigation process.

Additionally, Figures 12 and 13 show the elapsed time and corresponding wheelchair speed at various interval points along the trajectory from point A to point E, using the $EKFWC$ model across different surface types. These figures demonstrate how the system adapts its velocity profile based on terrain conditions, ensuring smooth and efficient motion. The data underscores the $EKFWC$'s capability to regulate speed dynamically while maintaining trajectory stability on smooth, uneven, and rough surfaces.

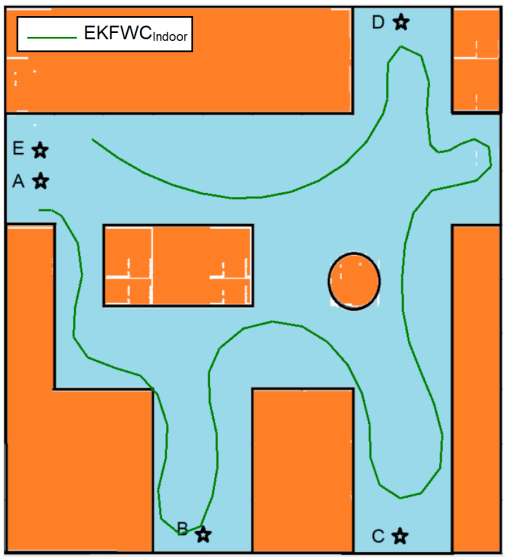

(a) Using $EKFWC$ in an indoor smooth surface

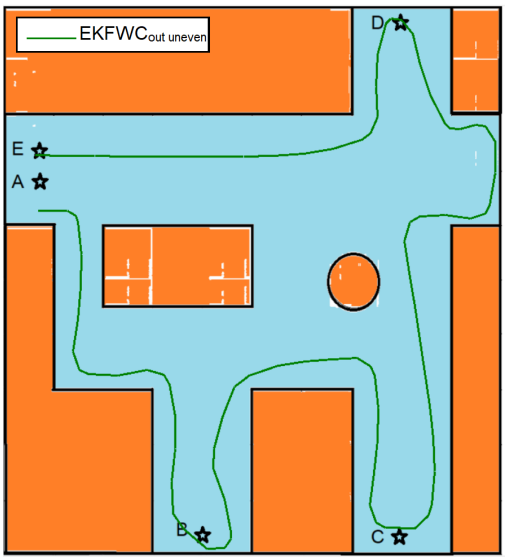

(b) Using $EKFWC$ in an outdoor uneven

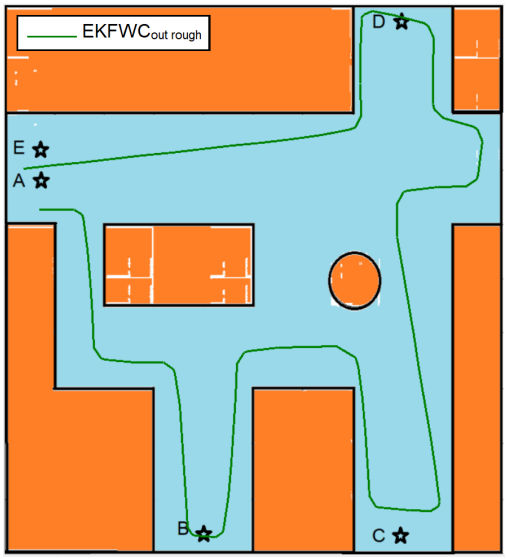

(c) Using $EKFWC$ in an outdoor very rough surface

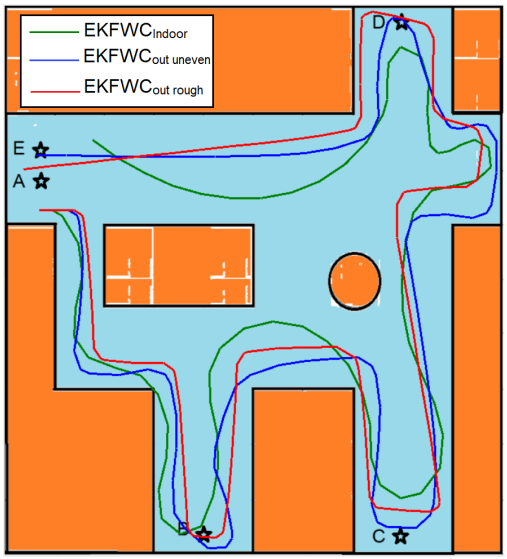

(d) Using $EKFWC$ on three surfaces

Figure 6: Using $EKFWC$ on Various surfaces

The proposed $EKFWC$ system significantly outperformed the reference model REF_{EKFPF} in terms of navigation time across various terrain types. Specifically, during indoor navigation on a smooth surface, the REF_{EKFPF} required 100 sec to traverse from point A to point E, while the $EKFWC$ completed the same path in a reduced time of 71 sec, demonstrating both faster and more efficient maneuverability. Furthermore, under outdoor conditions, $EKFWC$ maintained superior performance, completing the navigation

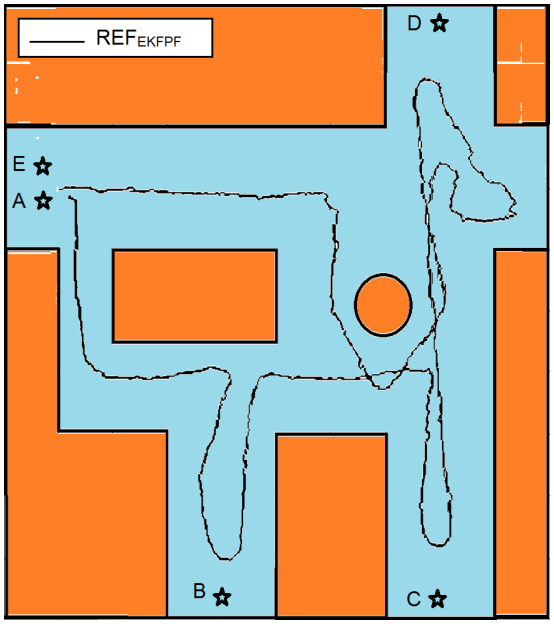

Figure 7: REF_{EKFPF} reference model navigation in the terrain

in 87 sec on uneven surfaces and 95 sec on very rough terrain. These results highlight the robustness and adaptability of the $EKFWC$ system across different environmental conditions.

Table 14 provides a detailed performance comparison between the proposed Enhanced Kalman Filter-based Wheelchair Control (EKFWC) model and the reference model, REF$_{\text{EKFPF}}$, which combines an Extended Kalman Filter with a Particle Filter. The comparative results clearly highlight the superior performance of the EKFWC model across all evaluated metrics and operational scenarios. Beginning with traversal time, the EKFWC model achieved significantly faster completion rates across varied terrain types. Specifically, it demonstrated up to 29% improvement in speed compared to the REF$_{\text{EKFPF}}$, indicating a more efficient response in both indoor and outdoor navigation tasks. This acceleration in traversal was consistently observed on all tested surfaces, ranging from smooth indoor flooring to more challenging rough outdoor paths. In terms of terrain adaptivity, the difference between the two models becomes even more evident. The reference REF$_{\text{EKFPF}}$ model applied a uniform control strategy regardless of terrain type, resulting in suboptimal handling on surfaces that deviate from ideal conditions. Conversely, the EKFWC model introduced an adaptive control strategy based on terrain classification. It incorporated three preset terrain profiles—smooth indoor, uneven outdoor, and rough outdoor—which allowed it to dynamically tune its estimation and control parameters in response to real-time environmental conditions. Moreover, the EKFWC model is designed with extensibility in mind, offering the flexibility for users to define and configure additional terrain types as needed, thus enhancing personalization and environmental responsiveness. With regard to noise filtering and signal correction, the EKFWC model exhibited superior performance. The robustness in noise handling

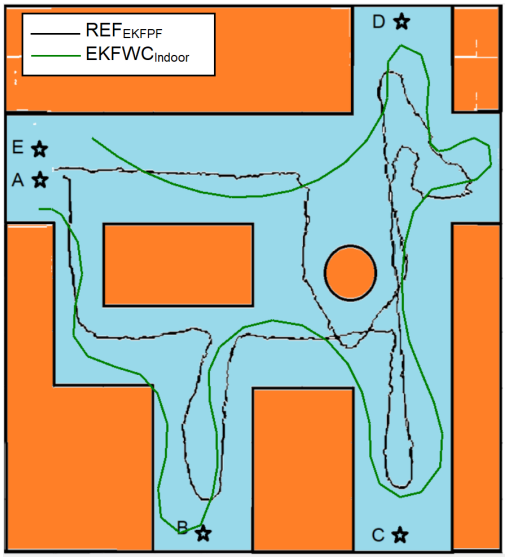

(a) $EKFWC$ vs REF_{EKFPF} in an indoor smooth surface

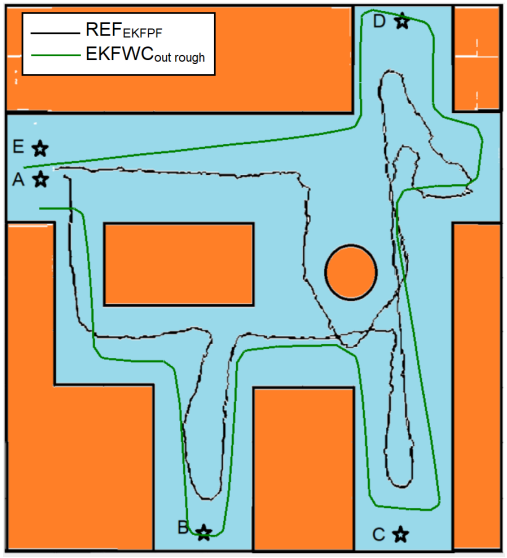

(b) $EKFWC$ vs REF_{EKFPF} in an Outdoor uneven surface

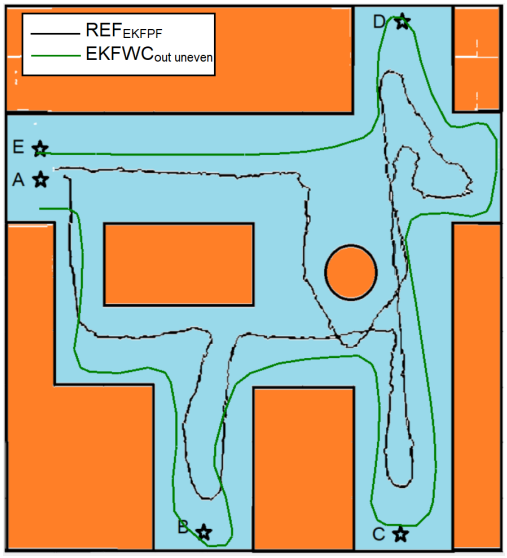

(c) $EKFWC$ vs REF_{EKFPF} in an outdoor very rough surface

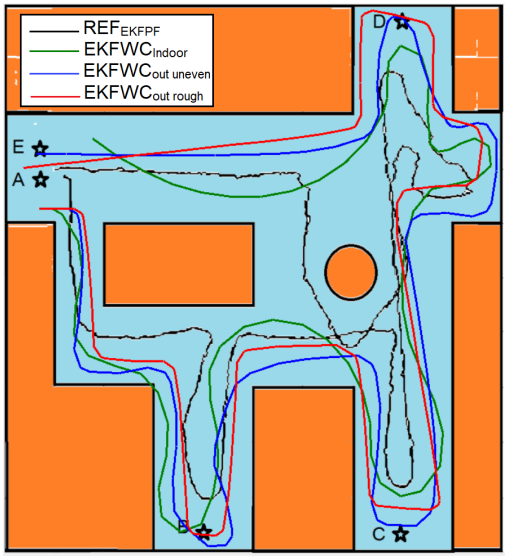

(d) $EKFWC$ vs REF_{EKFPF} on various surfaces

Figure 8: $EKFWC$ vs REF_{EKFPF} for various scenarios

can be attributed to its terrain-specific Kalman filter tuning, which optimizes estimation accuracy by taking into account the expected dynamics and noise characteristics of each terrain. This contrasts with the REF$_{EKFPF}$ model, which employs a general-purpose filtering approach not tailored to specific terrain types. The EKFWC model also showed greater robustness when deployed in real-world scenarios. Its dual-profile system for in-

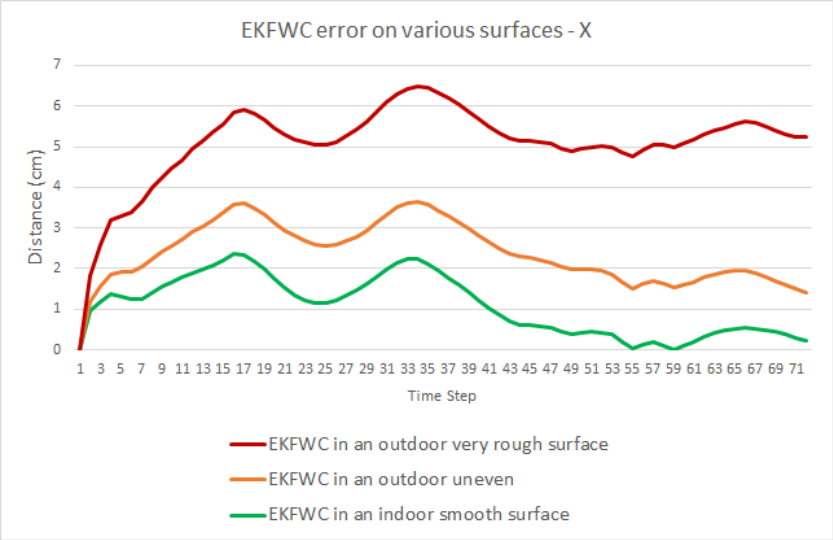

Figure 9: $EKFWC$ error in X for various surfaces

door and outdoor operation ensures that it maintains optimal performance under varied lighting, surface friction, and motion dynamics. This adaptability allows it to better accommodate the unpredictable nature of everyday environments, making it more practical for real users. Under the stability assessment criteria, the EKFWC model demonstrated notably smoother velocity and angular rate trajectories. Unlike the $\text{REF}_{\text{EKFPF}}$, which exhibited occasional instability manifested as sharp spikes or jitter in its motion profile, the EKFWC maintained continuous and stable control outputs. This smoothness not only enhances ride comfort but also reduces the likelihood of triggering corrective actions or system resets, thereby contributing to safer and more reliable wheelchair operation.

Table 14: Performance comparison

Metric	$EKFWC$ **(Proposed)**	REF_{EKFPF} **(Hybrid Filter)**	$EKFWC$ **Advantage**
Traversal Time	71s (Indoor Smooth) 87s (Outdoor Uneven) 95s (Very Rough)	100s (Indoor Smooth) 97s (Outdoor Uneven) 106s (Very Rough)	Up to 29% faster; quicker across all surfaces
Terrain Adaptivity	Explicit curves per surface; adaptive smoothing	Uniform treatment across terrains	Responsive to terrain changes; better alignment
Noise Filtering	Fast damping; smoother error across all axes	Moderate; filters encoder/laser noise only	Stronger filtering and correction
Real-World Robustness	Surface-specific tuning boosts resilience	Sensor-sensitive; performance degrades	More robust in diverse outdoor/indoor settings
Stability	Smooth trends, quick recovery from error	Spikes and delayed stabilization	More stable with consistent dynamics

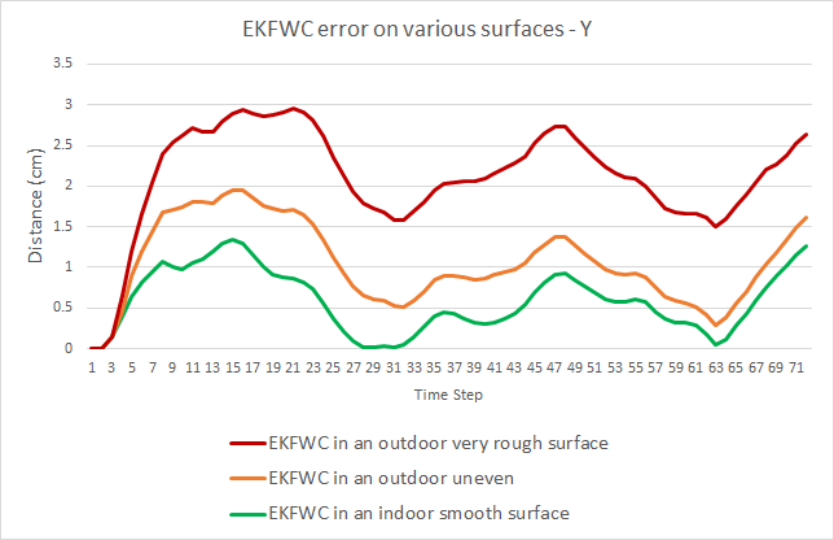

Figure 10: $EKFWC$ error in Y for various surfaces

The performance disparity is primarily attributed to the behavioral characteristics of the two control models. The reference model REF_{EKFPF} frequently deviated from the optimal trajectory, resulting in longer travel distances due to zigzag movements and wide turning angles. Additionally, it exhibited noticeable pauses and hesitation, particularly in response to terrain changes, which further contributed to increased traversal times. In contrast, the $EKFWC$ maintained a smoother trajectory with minimal deviation from the shortest path and showed a consistent response to terrain variations without incurring significant delays. This capability to maintain stable and continuous motion is a key advantage of the $EKFWC$, reflecting its effectiveness in real-time adaptive control and efficient path execution.

6. Conclusion and Future Work

The proposed $EKFWC$ system presents a significant advancement in intelligent wheelchair control for individuals with motor impairments, particularly those with cerebral palsy. By leveraging Kalman Filter-based state estimation and real-time velocity correction, $EKFWC$ effectively compensates for joystick input inaccuracies, resulting in smoother and more precise navigation. Simulation results show that EKFWC consistently outperforms the reference model REF_{EKFPF} across a variety of terrain conditions. Notably, When compared to REF_{EKFPF}, $EKFWC$ reduced navigation time from 100 sec to 71 sec on smooth indoor surfaces, and maintained superior performance on uneven and very rough outdoor terrain with traversal times of 87 sec and 95 sec, respectively. These improvements are attributed to $EKFWC's$ ability to maintain a stable trajectory with minimal deviations and prompt responses to terrain changes, avoiding the zigzagging and hesitations observed in the reference model. Overall, $EKFWC$ demonstrates robust adaptability, real-time responsiveness, and enhanced maneuverability in

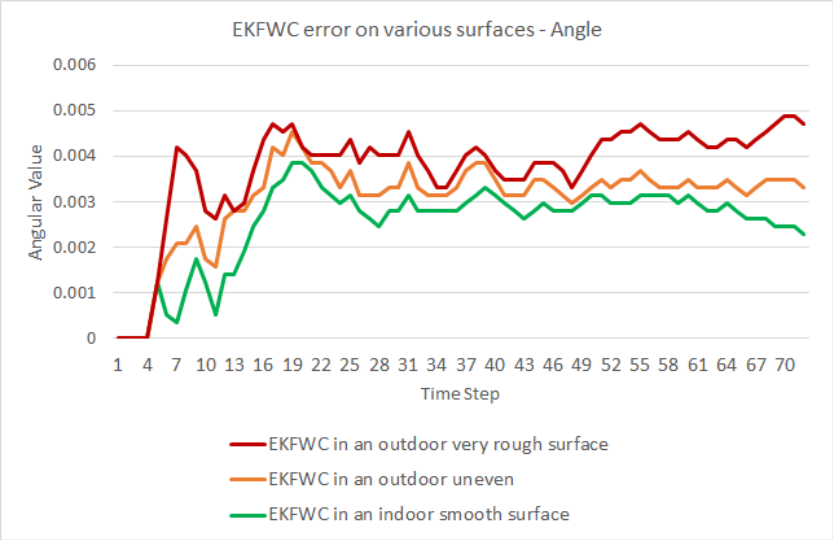

Figure 11: $EKFWC$ error in θ for various surfaces

diverse mobility environments.

Future work will focus on implementing the proposed $EKFWC$ system on a real electric wheelchair platform to validate its effectiveness beyond simulation. This includes integrating the control model with actual hardware components, such as joystick interfaces, motor drivers, and onboard sensors, to evaluate performance in real-time operation across diverse indoor and outdoor environments. Emphasis will be placed on testing the system with users who have motor impairments to assess its adaptability, reliability, and usability under real-world conditions. Additionally, further enhancements may involve adaptive tuning mechanisms to personalize the control response based on individual user behavior and dynamic terrain feedback, thereby improving overall system robustness and user experience.

References

[1] M. Babel, F. Pasteau, S. Guégan, P. Gallien, B. Nicolas, B. Fraudet, S. Achille-Fauveau, and D. Guillard. Handiviz project: Clinical validation of a driving assistance for electrical wheelchair. In *IEEE Workshop on Advanced Robotics and Its Social Impacts (ARSO)*, pages 1–6, Lyon, France, 2015.

[2] A. Kokosy, T. Floquet, G. Howells, H. Hu, M. Pepper, and C. Donz. An intelligent powered wheelchair. In *International Conference on Systems and Computer Science (ICSCS2012)*, Lille, France, 2012.

[3] R. Li, L. Wei, D. Gu, H. Hu, and K. McDonald-Maier. Multi-layered map based navigation and interaction for an intelligent wheelchair. In *Proceedings of IEEE International Conference on Robotics and Biomimetics (ROBIO)*, pages 115–120, Shenzhen, China, 2013.

[4] S.P. Levine, D.A. Bell, L.A. Jaros, R.C. Simpson, Y. Koren, and J. Borenstein. The

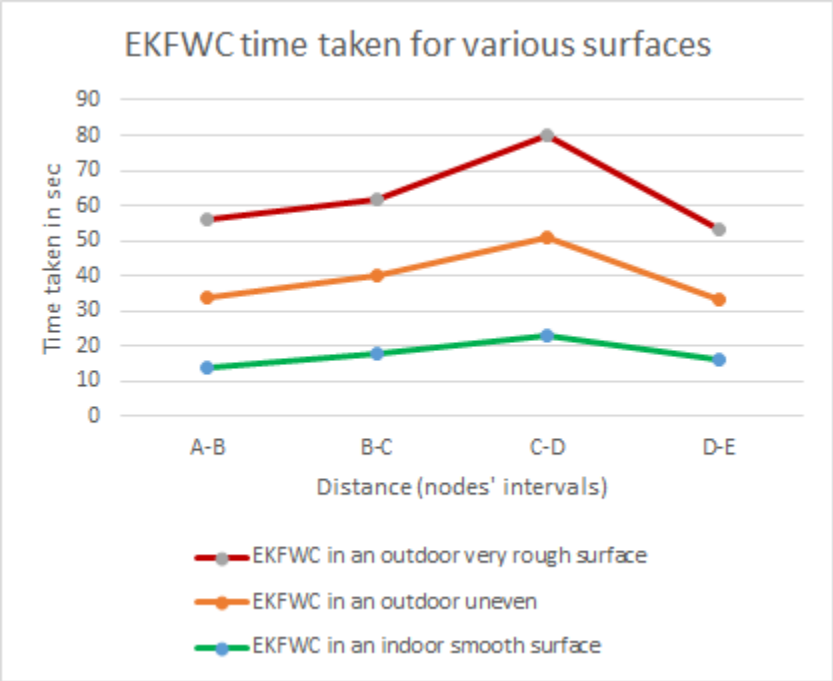

Figure 12: $EKFWC$ error in Y for various surfaces

navchair assistive wheelchair navigation system. *IEEE Transactions on Rehabilitation Engineering*, 7(4):443–451, 1999.

[5] E. Demeester, E. Vander Poorten, A. Huntemann, and J. De Schut. Wheelchair navigation assistance in the fp7 project radhar: Objectives and current state. In *IEEE/RSJ International Conference on Intelligent Robots and Systems (IROS), Workshop on Navigation and Manipulation Assistance for Robotic Wheelchairs*, Vilamoura, Portugal, October 2012.

[6] Khaled Safi, Wael Hosny Fouad Aly, Hassan Kanj, Tarek Khalifa, Mouna Ghedira, and Emilie Hutin. Hidden markov model for parkinson's disease patients using balance control data. *Bioengineering*, 11(1):88, 2024.

[7] Hassan Kanj, Ajla Kulaglic, Wael Hosny Fouad Aly, Mutaz AB Al-Tarawneh, Khaled Safi, Sawsan Kanj, and Jean-Marie Flaus. Agent-based risk analysis model for road transportation of dangerous goods. *Results in Engineering*, 25:103944, 2025.

[8] Hassan Kanj, Wael Hosny Fouad Aly, and Sawsan Kanj. A novel dynamic approach for risk analysis and simulation using multi-agents model. *Applied Sciences*, 12(10):5062, 2022.

[9] Mutaz AB Al-Tarawneh, Hassan Kanj, and Wael Hosny Fouad Aly. An integrated mcdm framework for trust-aware and fair task offloading in heterogeneous multi-provider edge-fog-cloud systems. *Results in Engineering*, page 105228, 2025.

[10] Wael Hosny Fouad Hosny Fouad Aly, Hassan Kanj, Nour Mostafa, Zakwan Al-Arnaout, and Hassan Harb. No binding machine learning architecture for sdn

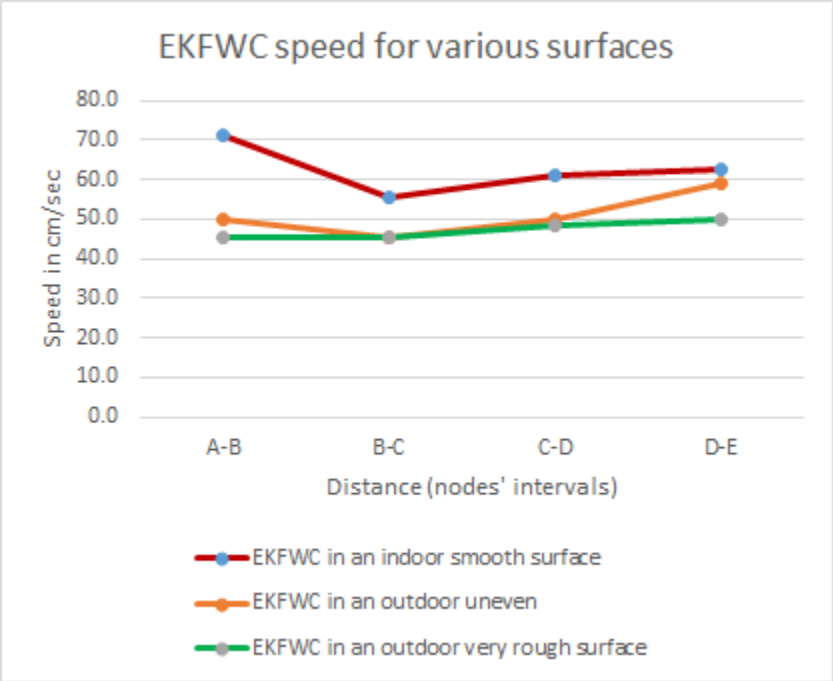

Figure 13: $EKFWC$ error in θ for various surfaces

controllers. *Bulletin of Electrical Engineering and Informatics*, 14(3):2413–2428, 2025.

[11] Wael Hosny Fouad Aly, Hassan Kanj, Samer Alabed, Nour Mostafa, and Khaled Safi. Dynamic feedback versus varna-based techniques for sdn controller placement problems. *Electronics*, 11(14):2273, 2022.

[12] Kassem Danach, Hassan Harb, Ameer Sardar Kwekha Rashid, Mutaz AB Al-Tarawneh, and Wael Hosny Fouad Aly. Location planning techniques for internet provider service unmanned aerial vehicles during crisis. *Results in Engineering*, 25:103833, 2025.

[13] Samer Alabed, Nour Mostafa, Wael Hosny Fouad Aly, and Mohammad Al-Rabayah. A low complexity distributed differential scheme based on orthogonal space time block coding for decode-and-forward wireless relay networks. *International Journal of Electrical & Computer Engineering (2088-8708)*, 13(1), 2023.

[14] Mutaz AB Al-Tarawneh, Omar Al-irr, Khaled S Al-Maaitah, Hassan Kanj, and Wael Hosny Fouad Aly. Enhancing fake news detection with word embedding: A machine learning and deep learning approach. *Computers*, 13(9):239, 2024.

[15] Ibrahim Mahariq, Ibrahim H Giden, Shadi Alboon, Wael Hosny Fouad Aly, Ahmed Youssef, and Hamza Kurt. Investigation and analysis of acoustojets by spectral element method. *Mathematics*, 10(17):3145, 2022.

[16] J. Leaman and H.M. La. A comprehensive review of smart wheelchairs: Past, present, and future. *IEEE Transactions on Human-Machine Systems*, 47(4):486–499, 2017.

[17] M. Dahmani, M.E.H. Chowdhury, A. Khandakar, T. Rahman, K. Al-Jayyousi, A. Hefny, and S. Kiranyaz. An intelligent and low-cost eye-tracking system for motorized wheelchair control. *Sensors*, 20(14):3936, 2020.

[18] A. Lankenau and T. Röfer. A versatile and safe mobility assistant. *IEEE Robotics & Automation Magazine*, 8(1):29–37, 2001.

[19] E. Prassler, J. Scholz, and P. Fiorini. A robotics wheelchair for crowded public environment. *IEEE Robotics & Automation Magazine*, 8(1):38–45, 2001.

[20] G. Bourhis, O. Horn, O. Habert, and A. Pruski. The vahm project: Autonomous vehicle for people with motor disabilities. *IEEE Robotics and Automation Magazine*, 7(1):21–28, 2001.

[21] B. Rebsamen, E. Burdet, C. Guan, H. Zhang, C.L. Teo, Q. Zeng, M. Ang, and C. Laugier. A brain controlled wheelchair based on p300 and path guidance. In *First IEEE/RAS-EMBS International Conference on Biomedical Robotics and Biomechatronics, BioRob 2006*, pages 1101–1106, Pisa, Italy, 2006.

[22] M. Mazo, J.C. García, F.J. Rodríguez, J. Ureña, J.L. Lázaro, and F. Espinosa. Integral system for assisted mobility. *Information Sciences*, 129(1-4):1–15, 2000.

[23] Y. Wang, W.D. Chen, and J.C. Wang. Hybrid map-based navigation for intelligent wheelchair. In *2011 IEEE International Conference on Robotics and Automation*, pages 637–642, Shanghai, China, 2011.

[24] X. Zhang, J. Li, L. Jin, J. Zhao, Q. Huang, Z. Song, X. Liu, and D.B. Luh. Design and evaluation of the extended fbs model based gaze-control power wheelchair for individuals facing manual control challenges. *Sensors*, 23(12):5571, 2023.

[25] A. Ravankar, A.A. Ravankar, Y. Kobayashi, Y. Hoshino, and C.C. Peng. Path smoothing techniques in robot navigation: State-of-the-art, current and future challenges. *Sensors*, 18(9):3170, 2018.

[26] Chadi F Riman and Wael HF Aly. Feedback control using arma to maneuver wheelchairs. *International Journal of Mechanical Engineering and Robotics Research*, 14(3), 2025.

[27] B. Muangmeesri and K. Wisaeng. Iot-based discomfort monitoring and a precise point positioning technique system for smart wheelchairs. *Applied System Innovation*, 5(5):103, 2022.

[28] A. Gasparri, S. Panzieri, F. Pascucci, and G. Ulivi. A hybrid active global localisation algorithm for mobile robots. In *Proceedings of the IEEE International Conference on Robotics and Automation (ICRA)*, pages 3148–3153, Rome, Italy, 2007.

[29] A. Achroufene, Y. Amirat, and A. Chibani. Rss-based indoor localization using belief function theory. *IEEE Transactions on Automation Science and Engineering*, 16(3):1163–1180, 2019.

[30] Y. Hao, A. Xu, X. Sui, and Y. Wang. A modified extended kalman filter for a two-antenna gps/ins vehicular navigation system. *Sensors*, 18(11):3809, 2018.

[31] Wael Hosny Fouad Aly. Lbftfb fault tolerance mechanism for software defined networking. In *2017 International Conference on Electrical and Computing Technologies and Applications (ICECTA)*, pages 1–5. IEEE, 2017.

[32] Wael Hosny Fouad Aly, Hassan Kanj, Nour Mostafa, and Samer Alabed. Feedback arma models versus bayesian models towards securing openflow controllers for sdns. *Electronics*, 11(9):1513, 2022.

[33] R. E. Kalman. A new approach to linear filtering and prediction problems. *Journal of Basic Engineering*, 82(1):35–45, 1960.

[34] W. Travis, A. T. Simmons, and D. M. Bevly. Corridor navigation with a lidar/ins kalman filter solution. In *IEEE Intelligent Vehicles Symposium*, pages 343–348, Las Vegas, NV, USA, 2005.

[35] Y. Bulut, D. Vines-Cavanaugh, and D. Bernal. Process and measurement noise estimation for kalman filtering. In T. Proulx, editor, *Structural Dynamics, Volume 3*, Conference Proceedings of the Society for Experimental Mechanics Series, pages 325–332. Springer, New York, NY, 2011.

[36] Wassila Meddeber, Benaoumeur Aour, and Karim Labadi. Smart wheelchair localization and navigation based on multi-sensor data fusion using hybrid-filter method (hf). *Revue d'Intelligence Artificielle*, 38(2), 2024.

[37] Sebastian Thrun. Probabilistic robotics. *Communications of the ACM*, 45(3):52–57, 2002.

[38] Karl Iagnemma and Steven Dubowsky. *Mobile robots in rough terrain: Estimation, motion planning, and control with application to planetary rovers*, volume 12. Springer Science & Business Media, 2004.

[39] Rudy Negenborn. Robot localization and kalman filters. *Utrecht Univ., Utrecht, Netherlands, Master's thesis INF/SCR-0309*, 2003.

[40] Timothy D Barfoot. *State estimation for robotics*. Cambridge University Press, 2024.